Research Article Vol. 14, No. 4 / 1 Apr 2023 / Biomedical Optics Express 1703
Biomedical Optics EXPRESS

Quantifying the drug response of patient-derived organoid clusters by aggregated morphological indicators with multi-parameters based on optical coherence tomography

LINYI ZHANG,[1] LING WANG,[1,2,4] SHANSHAN YANG,[1,2] KANGXIN HE,[3] DI BAO,[1] AND MINGEN XU[1,2,5]

[1]*Hangzhou Dianzi University, Automation College, Hangzhou, Zhejiang, China*
[2]*Zhejiang Provincial Key Laboratory of Medical Information and Biological 3D Printing, Hangzhou, Zhejiang, China*
[3]*First Affiliated Hospital, School of Medicine, Zhejiang University, Hangzhou, Zhejiang, China*
[4]*lingw@hdu.edu.cn*
[5]*xumingen@hdu.edu.cn*

Abstract: Patient-derived organoids (PDOs) serve as excellent tools for personalized drug screening to predict clinical outcomes of cancer treatment. However, current methods for efficient quantification of drug response are limited. Herein, we develop a method for label-free, continuous tracking imaging and quantitative analysis of drug efficacy using PDOs. A self-developed optical coherence tomography (OCT) system was used to monitor the morphological changes of PDOs within 6 days of drug administration. OCT image acquisition was performed every 24 h. An analytical method for organoid segmentation and morphological quantification was developed based on a deep learning network (EGO-Net) to simultaneously analyze multiple morphological organoid parameters under the drug's effect. Adenosine triphosphate (ATP) testing was conducted on the last day of drug treatment. Finally, a corresponding aggregated morphological indicator (AMI) was established using principal component analysis (PCA) based on the correlation analysis between OCT morphological quantification and ATP testing. Determining the AMI of organoids allowed quantitative evaluation of the PDOs responses to gradient concentrations and combinations of drugs. Results showed that there was a strong correlation (correlation coefficient >90%) between the results using the AMI of organoids and those from ATP testing, which is the standard test used for bioactivity measurement. Compared with single-time-point morphological parameters, the introduction of time-dependent morphological parameters can reflect drug efficacy with improved accuracy. Additionally, the AMI of organoids was found to improve the efficiency of 5-fluorouracil(5FU) against tumor cells by allowing the determination of the optimum concentration, and the discrepancies in response among different PDOs using the same drug combinations could also be measured. Collectively, the AMI established by OCT system combined with PCA could quantify the multidimensional morphological changes of organoids under the drug's effect, providing a simple and efficient tool for drug screening in PDOs.

1. Introduction

Patient-derived organoids (PDOs) as *in vitro* organotypic models which can stably reproduce morphological characteristics and some physiological functions of the original healthy tissues have gained enormous interest in personalized medicine, drug screening, and cell therapy [1]. Since PDOs achieve to predict drug response due to their inherent ability in preserving the heredity and heterogeneity of original tumors, offering an excellent tool for high-throughput drug screening and drug toxicity assessment [2,3]. Current PDOs, such as the gastrointestinal

#486666 https://doi.org/10.1364/BOE.486666
Journal © 2023 Received 31 Jan 2023; revised 17 Mar 2023; accepted 17 Mar 2023; published 29 Mar 2023

Biomedical Optics EXPRESS

tract, pancreas, liver, breast, prostate, and lung can be transferred, cryopreserved, and genetically altered for long periods and do not undergo any significant gene mutation or epigenetic changes [4,5]. PDOs which were extracted from different patients would indicate the incidence status of individuals. Therefore, a living biological database that contains overall information about various patients would be formed, providing chemosensitivity data of individual patients for effective chemotherapy treatments [2]. However, the current evaluation method for achieving accurate drug response prediction using organoids are limited in clinical trials. Consequently, quantitative method for accessing drug efficacy is required for drug screening.

Current quantification of the PDO drug response is obtained by cell viability measurements, biochemical testing, expression of cell-specific labels or transgenic reporter genes and bright-field microscopy [6]. Biochemical testing approaches such as 3-(4,5-dimethylthiazol-2-yl)-2,5-diphenyltetrazolium bromide(MTT), adenosine triphosphate (ATP), 2, 3-bis (2-methoxy-4-nitro-5-sulfophenyl)-5-[(phenylamino) carbonyl]-2H-tetrazolium hydroxide(XTT), and cell counting kit-8(CKK-8) are usually destructive which fails to monitor organoids over long periods [7–11]. Other methods used for the morphological observation of organoids, such as histological staining, fluorescence microscopy, and bright-field microscopy, usually lack the ability to image volumetric structures. Ultimately, this may lead to large errors in quantitative analysis that is based on 2D information or the approximation of organoids as spheres or ellipsoids [12]. Therefore, a monitoring tool that enables the continuous and non-destructive three-dimensional (3D) imaging of organoids over a relatively short period is urgently needed to evaluate the growth and drug responses of organoids.

Optical coherence tomography (OCT) is a non-invasive 3D image technique with high spatial resolution [13]. The millimeter-scale penetration depth and micrometer-scale resolution of OCT enable this technique to depict the internal structures of organoids with high resolution. Furthermore, the label-free nature of OCT allows the longitudinal monitoring of quantitative and morphological variation in these organoids. Deloria et al. adopted 3D OCT with ultra-high resolution to observe the internal structures of trophoblastic organoids derived from human placenta [14]. Ming et al. utilized a spectral-domain optical coherence tomography (SD-OCT) system to characterize the growth of cardiac organoids derived from human pluripotent stem cells, ultimately observing the complex connections between cavities of different sizes [15]. Additionally, Gil et al. introduced an OCT method to track the volumetric growth of colorectal cancer PDOs, preliminarily verifying the feasibility of OCT in evaluating organoid drug responses [16]. It is important to note that PDOs as 3D *in vitro* model for drug screening exhibit more morphological indicators besides volume value. Consequently, quantification analysis which only considering organoid volume would lead to more biased evaluation of organoid drug responses, whereas the characterization of multiple morphological indicators would facilitate a more comprehensive and accurate evaluation of organoid growth [16–18].

To improve the development of drug therapeutic schemes for cancer, a self-developed SD-OCT system was adopted to monitor the morphological variations in PDOs across a 6-day treatment protocol with different drugs. Moreover, combining a deep learning network (EGO-Net) for organoid segmentation and morphological quantification with principal component analysis (PCA) would allow the aggregated morphological indicator (AMI) method established, which could quantitatively evaluate drug efficacy in individual patients. Furthermore, ATP testing was adopted to measure organoid viability. Finally, the correlation between the result of ATP testing and AMI results was used to evaluate the accuracy and effectiveness of AMI method in analyzing personalized antineoplastic efficacy *in vitro*.

Biomedical Optics EXPRESS

2. Methods

2.1. Culture and dosing of patient-derived colorectal cancer tissue

Colorectal cancer organoids were derived from three patients (Patient1(P1), Patient2(P2), and Patient3(P3)). The organoids used for drug screening require the observable budding of organoids under bright-field microscope (4× magnification), and most of the organoids have the actual equivalent diameter of no less than 50 μm. PDOs for the drug sensitivity assay were cultured in 96-well plates. One 96-well plate was used per patient for a total of three 96-well plates. The drug concentration gradients and drug combination schemes used were designed in advance. The concentration gradient of the antineoplastic drug 5-fluorouracil (5-FU) and dosing scheme of different drug combination were shown in Table 1 and Table 2, respectively. Three wells were cultivated for each concentration or drug combination. A volume ratio of Matrigel: cell suspension of 2:1 was used during organoid culture, with medium changed every 48 h. Observation was conducted with an optical microscope every 24 h, and data were acquired every 24 h by OCT. ATP testing was conducted on the final day (day 6).

Table 1. Gradient concentration dosing of organoid samples.

Serial number	Drug name	Type of medication	Drug concentration
1	Control (No treatment)	n/a	n/a
2	5FU (5fluorouracil) [4]	Anti-metabolic drugs	$5\mu g/ml$
3			$15\mu g/ml$
4			$45\mu g/ml$
5			$135\mu g/ml$
6			$405\mu g/ml$

Table 2. Addition of drug combinations in organoid samples.

Serial number	Drug name	Type of medication	Drug concentration
1	Control (No treatment)	n/a	n/a
2	5FU [4]	Anti-metabolic drugs	$5\mu g/ml$
3	Trastuzumab [19]	Targeted agents	$175\mu g/ml$
4	Vemurafenib [20]	Protein inhibitors	$21.014\mu g/ml$
5	FOLFIRI combination [21]	Combination medication	5FU:$22.5\mu g/ml$ SN38 :$0.014\mu g/ml$
6	Cetuximab with Vemurafenib [22]	Drug combinations	Cetuximab: $0.087\mu g/ml$ Vemurafenib:$21.014\mu g/ml$

2.2. OCT imaging

High-resolution SD-OCT, with a central wavelength of 1310 nm and a full width at half maximum of 248 nm, was employed to acquire organoid data (Fig. 1). The axial and lateral resolutions of the OCT system were 4.6 μm (in air) and 13 μm, respectively. The imaging depth was 3.5 mm, and the A-Scan scanning frequency was set to 48 kHz. 3D OCT images of $4 \times 4 \times 3.58$ mm (800 (x) × 800 (y) × 1024 (z) $pixels$) were obtained with a sensitivity of 111 dB and pixels measuring 5(x) × 5 (y) × 3.49 (z) μm.

2.3. ATP viability measurement of organoids

ATP as the main energy currency of cell which can be used to reflect the metabolic activity of a cell. ATP content which considered as the standard for bioactivity quantification is one of the

Biomedical Optics EXPRESS

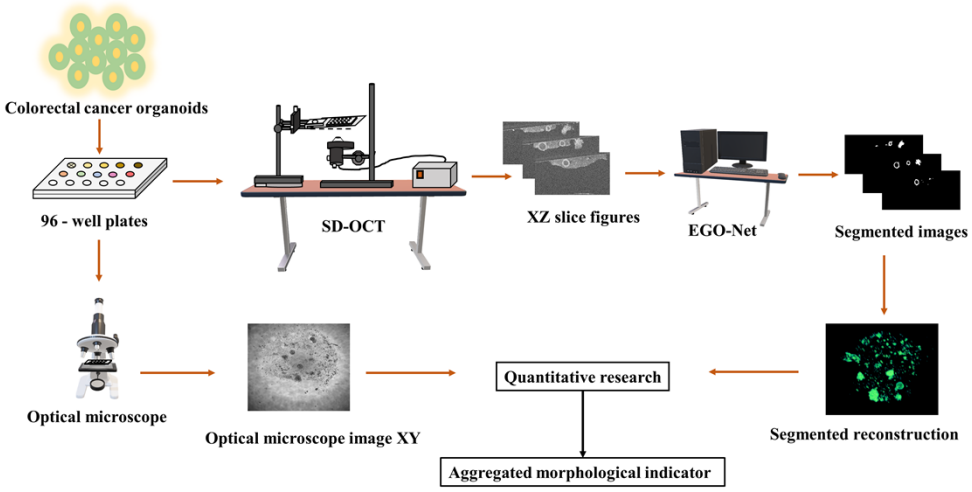

Fig. 1. Colorectal cancer organoid collection and data processing process. Patient-derived colorectal cancer organoids in 96-well plates were treated with drugs. Different colors represented different dosing schemes. SD-OCT data was acquired every 24 hours, and photos were taken by bright-field microscope after each SD-OCT acquisition. The SD-OCT images were segmented by self-designed EGO-Net network and reconstructed for the organoid's quantification. After statistical processing, organoids AMIs were finally obtained.

most common methods used in antineoplastic drug screening [23]. In this study, the ATP value was obtained via chemiluminescence analysis of colorectal cancer organoids that were cultured and treated with various drugs in 96-well plates for 6 d [24].

2.4. Morphological quantification of organoids

The OCT images were subjected to pre-processing and accurate target organoid segmentation to achieve precise assessment of the organoids morphological characteristics [25,26]. Given the fact that OCT images would exhibit several problems hampering precise organoids segmentation, such as the morphological diversity of organoids and low contrast between organoids and surrounding medium, we designed an EGO-Net network to enhance the organoid boundaries recognition which allow accurate segmentation of the target organoids. The image process of organoids was shown in Fig. 2(A-F). It was reported that the recognition accuracy of this network could reach 85.4% [34] for organoids with an equivalent diameter $\geq$32 μm [27,28]. The volume, surface area, sphericity, quantity, and other morphological parameters of the separated organoids were quantified based on the connected-region calculation. The daily mean value and inter-day standard deviation for the organoid morphological parameters were used as quantification indicators of temporal fluctuation. Figure 2(G) shows the morphological index quantification process of organoids. The quantification algorithm used to analyze the organoid morphological parameters is shown in Algorithm 1.

2.5. Analysis of the AMI of the organoids

The AMI of the organoids was obtained based on the statistical correlation between the single organoid morphological parameters and the ATP test results. Considering the limitations in terms of sample quantity, Spearman correlation analysis was performed between each morphological parameter and the ATP test results. Morphological parameters that showed strong correlation with organoid viability (Spearman correlation coefficient > 0.85), were selected for further analysis. Screening indicators were then adjusted using PCA to obtain the AMI of organoids.

Biomedical Optics EXPRESS

Algorithm 1. Morphological quantification of organoids

1 Png format images were saved as mat format data.
2. Holes in each frame of X-Z images (imfill option = "holes") were filled and saved as 3D filled image data.
3. Image data with filled holes were used to obtain the 3D boundary image data.
4. Connected regions in 3D filled image data (bwlabeln) were labelled and the actual pixel quantity in each connected region (regionprops = "Area") counted. The index subscript of regional pixels was saved (regionprops = "PixelIdxLis").
5. Voxels, filled voxels, and surface area pixels in each connected region were calculated.
6. Actual voxels and surface area pixels were calculated (actual 3D pixel size = $5 \times 5 \times 3.49$(z) μm^3, actual 2D pixel size = 5×5 μm^2).
7. The connected regions of organoids with equivalent diameters < 32 μm were eliminated [16].
8. For organoids with equivalent diameters ≥32 μm, the equivalent diameter, quantity, overall volume, overall surface area, and specific surface area in each well were calculated along with the average volume, average specific surface area, and average sphericity of the individual organoids.
9. The daily mean value and inter-day standard deviation for each organoid morphological parameter, such as the overall volume, the overall surface area in a single well, were calculated for each cell.

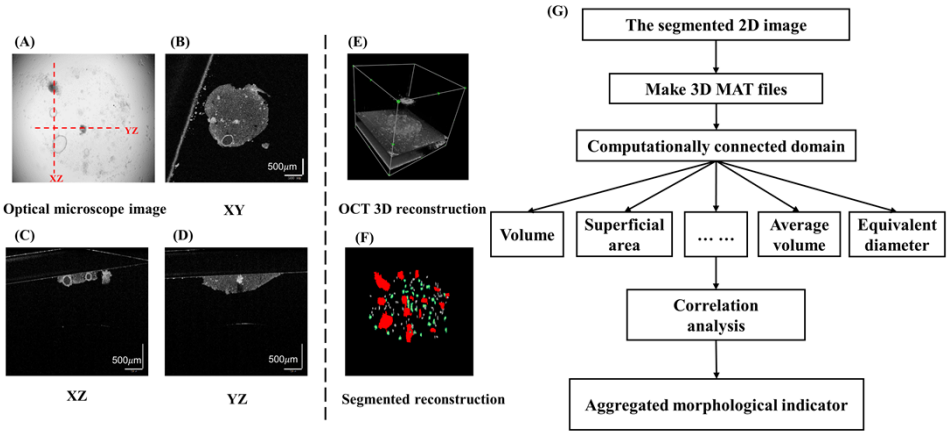

Fig. 2. Image processing process and morphological index quantification process of organoids. A: organoid image captured by optical microscope. B-D: OCT images of three sections, namely XY, XZ, and YZ sections. E: 3D OCT original image reconstruction. F: 3D segmentation image reconstruction. G: Quantification process of organoid morphological parameters. Scale bar = 500μm.

(1) Establishment of standardized morphological parameter Matrix A for organoids by PCA: The PCA method requires the elimination of various dimensions effects in the morphological parameters. The Z-Score method was adopted to standardize the morphological parameters selected by Spearman correlation analysis. Consequently, the standardized morphological

Biomedical Optics EXPRESS

parameter Matrix A of organoids was established as follows:

$$A = \begin{bmatrix} x_{11} & x_{12} & \cdots & x_{1j} & \cdots & x_{1l} \\ x_{21} & x_{22} & \cdots & x_{2j} & \cdots & x_{2l} \\ \cdots & \cdots & \cdots & x_{ij} & \cdots & \cdots \\ x_{m1} & x_{m2} & \cdots & x_{mj} & \cdots & x_{ml} \end{bmatrix}, \tag{1}$$

Matrix A is an array with m rows and l columns, where m is the overall number of culture wells used in the three 96-well plates, l is the number of morphological parameters, and x_{ij} is the value of the j_{th} morphological parameter in the i_{th} culture well. In this study, $m = 108$ *and* $l = 10$.

(2) Establishment of the morphological parameter polynomial F_{ik} for the organoids:

The weights of the organoid morphological parameters were calculated by singular value decomposition (SVD) and the organoid morphological parameters normalized according to their weight coefficients.

Firstly, the covariances between the organoid morphological parameters were calculated to establish covariance Matrix B with l rows and l columns.

$$B = cov(A),$$
$$B = \begin{bmatrix} cov(x_1, x_1), & cov(x_1, x_2) & \cdots & cov(x_1, x_j) \cdots & cov(x_1, x_l) \\ \vdots & & \ddots & & \vdots \\ cov(x_l, x_1), & cov(x_l, x_2) & \cdots & cov(x_l, x_j) \cdots & cov(x_l, x_l) \end{bmatrix}_{l \times l}, \tag{2}$$

In Matrix B, $cov()$ indicates covariance, and x_j indicates the j_{th} morphological parameter, $x_j = [x_{1j}, x_{2j}, \ldots, x_{mj}]^T$.

The eigenvalues and eigenvectors of the covariance matrix, calculated by SVD, formed an eigenvalue sequence from largest to smallest. The eigenvectors corresponding to the sorted eigenvalues were then used as weight coefficients for the organoid morphological parameters.

The eigenvalue λ_k in matrix $B^T B$ was then calculated:

$$|B^T B - \lambda_k E| = 0, \tag{3}$$

The eigenvector v_k that corresponds to eigenvalue λ_k was obtained by introducing eigenvalue λ_k into the following equation:

$$(B^T B - \lambda_k E) v_k = 0, \tag{4}$$

Eigenvectors were then sorted to form a sequence from large to small in terms of the eigenvalues λ_k. In the sequence, $v_k = [a_{k1}, a_{k2}, \ldots, a_{kl}]^T$ is the weight coefficient of the kth normalized organoid morphological parameter F_{ik} in the ith culture well. The normalized organoid morphological parameters, F_{ik}, were obtained by multiplying the standardized organoid morphological parameters with their weights, shown as follows:

$$F_{ik} = a_{k1} x_{i1} + a_{k2} x_{i2} + \ldots + a_{kj} x_{ij} + \ldots + a_{kl} x_{il} \tag{5}$$

(3) Acquisition of the AMI:

The AMI of the organoids was established according to the singular value proportion, that is, whether the value $\sum b_k$ exceeded threshold α (α = 85% in this study). The first three normalized polynomials from the organoid morphological parameters were selected, whose weights are the

Biomedical Optics EXPRESS

singular value proportions with the relationship $\sigma_k = \sqrt{\lambda_k}$ between the singular value σ_k and the eigenvalue λ_k.

$$b_k = \frac{\sigma_k}{\sum_{k=1}^{l} \sigma_k}, \tag{6}$$

$$\sum b_k > threshold\ \alpha, \tag{7}$$

The proportion of the singular value b_k is the variance contribution rate of the k_{th} normalized organoid morphological parameter F_{ik} (the weight of F_{ik}).

Finally, the weights of the normalized organoid morphological parameters in the ith culture well were multiplied by the polynomials of the normalized organoid morphological parameters in the ith culture well. The results were then summed to obtain the AMI of the organoids in the ith culture well, AMI:

$$AMI = \sum_{k=1}^{3} b_k F_{ik}, \tag{8}$$

2.6. Statistical analysis

Statistical product and service solutions (SPSS) was used for all statistical analyses. The average values from the repeated experiments were adopted for quantification of the organoid morphological parameters. And well replicates were applied to reduce random errors. The inter-day standard deviation of the organoid morphological parameters was used as the quantification indicator of temporal fluctuation in the morphological parameters. Spearman correlation coefficients were calculated for correlation analysis of the morphological parameters and ATP tests, with all selected indicators showing significant correlation ($P < 0.05$). The obtained Kaiser-Meyer-Olkin value > 0.7 in the PCA tests indicated that the PCA can be utilized for organoids to obtain the one-dimensional AMI. The principal components were selected when the cumulative variance contribution rate was $> 85\%$.

3. Result

3.1. Drug actions lead to various volumetric change rates in PDOs from different patients

The observation of volumetric change in different PDOs under same drug treatment would be beneficial to ascertain any differences between individuals. The organoids growth is a continuous process, where the quantitative analysis of the volumetric change rates for different drugs allows the identification of drugs with optimal efficacy and facilitate more personalized and precise treatment of patients [16]. The morphological images of the time-dependent changes in PDOs from P1 and P2 are shown in Fig. 3(A) (organoids with an equivalent diameter $< 32\ \mu m$ were eliminated). PDOs volume began to change significantly from the day 3. The organoid volume in each well was calculated and compared with the volume of the control group. The daily volume in each well required normalization because of discrepancies in the quantities of the initial organoids; this was conducted by dividing the volume observed on each day by the volume on the first day. The overall single-well volumetric change rates of the different drug-treated patient-derived colorectal cancer organoids compared to the control group is shown in Fig. 3(B), (C). The daily overall volumetric change rate was obtained by subtracting the normalized volume for the control group from that of the drug group. The drug responses of P1 and P2, who both suffered from colorectal cancer, were generally similar. An ascending trend of volume value was observed in both the trastuzumab-treated and vemurafenib-treated groups when compared with the control group, whereas a descending trend was seen in the other three groups. It should be noted that the overall organoid volume on the sixth day of drug effect resulted in a Spearman correlation coefficient < 0.8 when compared to the ATP tests results. This indicated a lack of accuracy when using a single organoid volume measurement to characterize drug response.

Biomedical Optics EXPRESS

Considering the time-dependent organoid volumetric change caused by drug treatment, the daily change and amplitude of time-dependent fluctuations in organoid volume were characterized by the corresponding daily mean value and rolling standard deviation in each individual organoid. Spearman correlation coefficients of 0.8403 and 0.8609 were obtained between ATP tests and the daily mean value and rolling standard deviation of the average volume in individual organoids, respectively; both correlations were considered statistically significant ($P < 0.01$). This result indicates a strong correlation between the time-dependent volumetric change and the bioactivity of organoids, showing quantification of the time-dependent changes in the organoid morphological parameters can more accurately reflect drug efficacy.

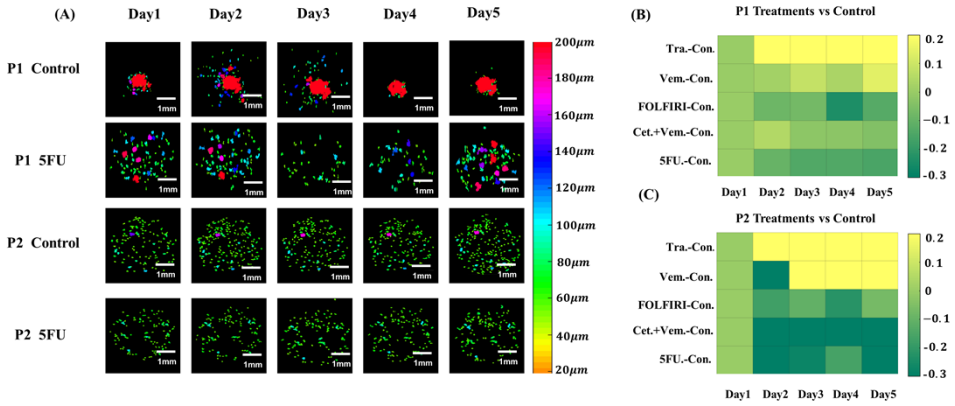

Fig. 3. Volume changes in patient-derived tumor organoids due to drug treatment. A: 3D OCT segmented images of different patient colorectal cancer organoids (control, 5FU-treated group), including. B-C: Heat map show pairwise differences of overall volume change between each treatment and control. Top: Colorectal cancer organoids from P1. Bottom: Colorectal cancer organoids from P2. Scale bar = 1mm.

3.2. *Quantification of time-dependent morphological parameters in organoid clusters cultured on individual well plates*

Previous studies have revealed that organoids are not perfect spheres and the drug effect efficacy on organoids cannot be accurately reflected by only quantifying time-dependent changes that occur in the organoid volume [18]. Due to discrepancies in the surface area and organoid sphericity, the trends in time-dependent changes of morphological parameters, such as volume, surface area, and sphericity, are not entirely consistent for each organoid. The time-dependent changes in the overall volume, overall surface area, and average sphericity of the organoids from P1 with no drug and 15 $\mu g/mL$ 5-FU treatment are shown in Fig. 4. These results indicate that similar time-dependent change trends for overall volume and surface area, whereas the changing trend in average sphericity is comparatively not obvious. Spearman correlation analysis between the morphological parameters and the ATP test results indicate organoid viability based on the morphological parameters of the PDOs from P1 and P2 under different drug treatments (Fig.S1). The quantitative AMI expression was established using PCA. Based on Spearman correlation analysis, the morphological parameters used to calculate the AMI were determined from the average surface area on the last day (ASA_{last}), the equivalent diameter on the last day (D_{last}), the daily mean average volume for a single organoid (AV_{mean}), the daily mean average surface area for a single organoid (ASA_{mean}), the daily mean average sphericity for a single organoid (ASP_{mean}), the daily mean equivalent diameter for a single organoid (D_{mean}), the rolling standard deviation in the daily change rate for the specific surface area in a single organoid (DSA_{std}),

Biomedical Optics EXPRESS

the rolling standard deviation for the average volume for a single organoid (AV_{std}), the rolling standard deviation for the average surface area for a single organoid (AS_{std}), and the rolling standard deviation for the equivalent diameter for a single organoid (D_{std}). Using SVD of the covariance matrix, the formula of the three normalized organoid morphological parameters with a variance ratio > 85% was obtained and is presented as follows:

$$F_1 = 0.3433ASA_{last} + 0.3291D_{last} + 0.3426AV_{mean} + 0.3450ASA_{mean} + 0.0537$$
$$ASP_{mean} + 0.3291D_{mean} + 0.2990DSA_{std} + 0.3392AV_{std} + 0.3347AS_{std} + 0.3312D_{std},$$
$$F_2 = -0.0373ASA_{last} + 0.1365D_{last} + 0.0108AV_{mean} - 0.0195ASA_{mean} + 0.9544$$
$$ASP_{mean} + 0.1620D_{mean} - 0.1064DSA_{std} - 0.0958AV_{std} - 0.1104AS_{std} - 0.0979D_{std},$$
$$F_3 = -0.2094ASA_{last} - 0.3551D_{last} - 0.2104AV_{mean} - 0.1704ASA_{mean} + 0.2308$$
$$ASP_{mean} - 0.2963D_{mean} + 0.6546DSA_{std} + 0.0888AV_{std} + 0.1388AS_{std} + 0.4000D_{std}$$

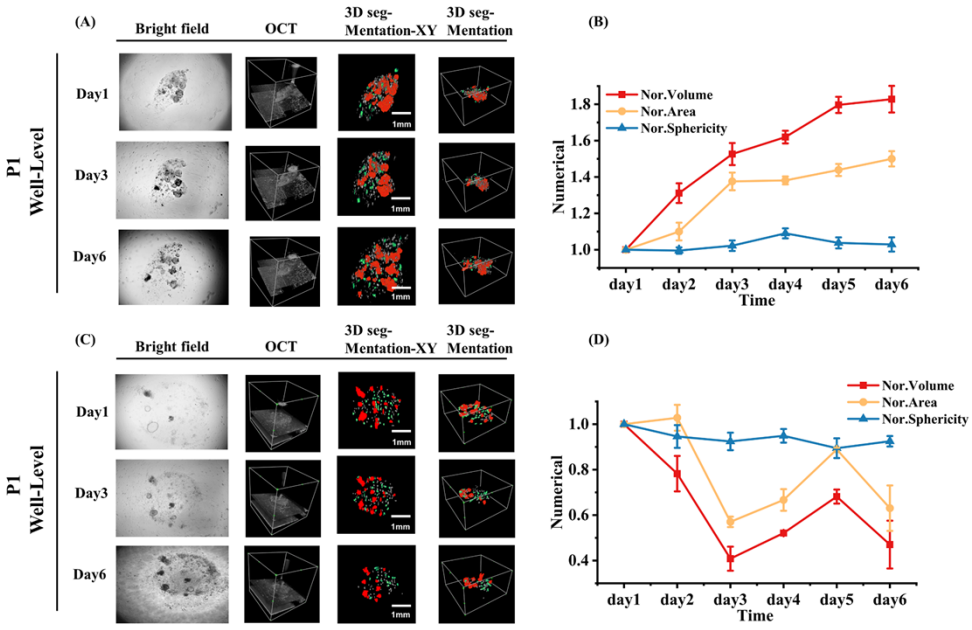

Fig. 4. Morphological tracking result of P1 PDOs. A: Bright field microscope, OCT and corresponding processing images under no treatment. B: Changes in overall organoid volume, overall surface area and mean sphericity under the no treatment. C: Bright field microscope, OCT and corresponding processing images under 5FU treatment. D: Changes in overall organoid volume, overall surface area and mean sphericity under 5FU treatment. (Error bars indicate standard deviation, n = 3).

On this basis, the normalized organoid morphological parameters were linearly weighted by PCA to construct an AMI for the organoids:

$$AMI = 0.825673F_1 + 0.103979F_2 + 0.043914F_3\ , \tag{9}$$

3.3. Testing drug efficacy over a concentration gradient based on AMI quantification

To test the correlation between the AMI and the ATP test results and determine the effects of drug delivery over a concentration gradient, 5-FU experiments were conducted on P1 PDOs. The

Biomedical Optics EXPRESS

specific concentrations used are listed in Table 1. OCT images and morphological quantification results of P1 PDOs under 5-FU treatment at different concentrations is shown in Fig. 5. As shown in Fig. 5(A), descending trends were observed in the P1 PDOs quantity under the different 5-FU concentrations. Meanwhile the volumes of single organoids and the overall volume of the organoids in a single well showed same trend. In contrast, the organoids number increased significantly over the first 3 days in the control group, with the overall volume of organoids showing the increased trend throughout the entire observation period.

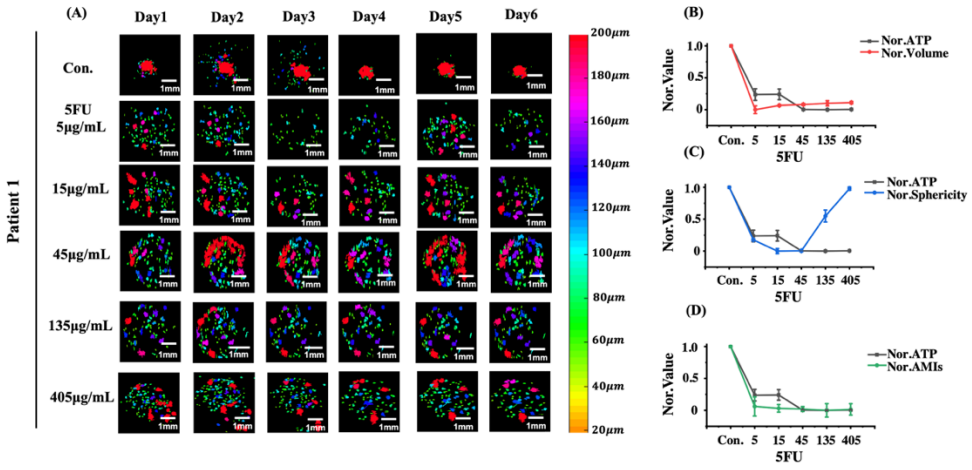

Fig. 5. OCT 3D segmentation and quantification results of P1 PDOs treated with different concentrations of 5FU. A: OCT segmentation images of P1 PDOs treated with gradient concentrations of 5FU drug, where different color bars represent different equivalent diameters of the organoid. B-D: ATP results versus mean volume, mean sphericity and AMIs results of organoids in the single well plate at different 5FU concentration. Scale bar = 1mm. (Error bars indicate standard deviation, n = 3).

The changes in average volume, average sphericity, AMIs, and ATP measurement across different 5-FU doses are shown in Fig. 5(B–D). To obtain more comparable correlations, each indicator in the figure was normalized against the results obtained for the control group. Normalization was performed by normalizing to the control group ($Nor.Value = \frac{value_{Drug}}{value_{Control}}$). As shown in Fig. 5(B–D), the average volume of all organoids decreased to a certain extent under 6 days of drug treatment at different concentrations when compared to those in the control group. However, this decrease was not sustained as the drug concentration increased, with a minimum organoid volume observed at a 5-FU concentration of 5 $\mu g/mL$. When the drug concentration exceeds 5 $\mu g/mL$, the normalized organoid average volume rebounds as the drug concentration increases. The average sphericity of organoids decreased to a minimum after 6 days of 15$\mu g/mL$ 5-FU treatment. Continuous increased drug concentration led to a significant rebound in the average sphericity of organoids, and the AMIs for P1 PDOs declined as the 5-FU concentration increased; these AMI results exhibited a significant similarity to the results of the ATP viability test. Overall, the drug efficacy assay results measured by AMI were consistent with the conclusion that the cancer cell killing efficiency can be enhanced by increasing the 5-FU concentration, as reported in other work [29]. This indicates that, compared with a single morphological indicator, the AMI of organoids contains multi-dimensional temporal and structural data, upon which drug efficacy can be better determined.

Biomedical Optics EXPRESS

3.4. Testing the efficacy of different drugs based on AMI quantification

To investigate the testing drug efficacy of AMI, combined drug experiments with different drug combinations were conducted on P3 PDOs without the use of PCA. The specific dosing scheme is listed in Table 2. Normalized morphological parameters of PDOs from P3 were introduced to Formula (9) to obtain the AMI under different drug treatments. OCT images were obtained from the continuous monitoring of P3 PDOs under the different drug treatments over 6 days (Fig. 6(A)). Based on the OCT segmentation images of the separated organoids, combined 5FU, SN38 treatment, combined cetuximab, vemurafenib treatment and 5-FU treatment reduced the quantity, size, and overall volume of the organoids in a single well. While no significant changes were observed occurred in the same parameters for the organoids in single wells under the vemurafenib effect alone. The tracking results for individual organoids, illustrated with white arrows in Fig. 6(A), were consistent with the overall drug response of these organoids. To eliminate additional dimensional effects, the morphological parameters from P3 PDOs and the ATP test results were normalized to the control group ($Nor.Value = \frac{value_{Drug}}{value_{Control}}$). When comparing the results of organoid morphological quantification with the ATP tests (Fig. 6(B–D)), inconsistency was observed between the ATP test results and the average volume and sphericity of P3 PDOs across the 6 days treatment. However, the obtained AMI results including the temporal and multi-dimension structural data, which were highly consistent with the ATP test results. The calculated Pearson correlation coefficient of the ATP results compared to the average volume, average sphericity, and AMI were 0.851 ($P < 0.05$), 0.018, and 0.925 ($P < 0.01$), respectively. The ATP test is considered the standard method in quantifying bioactivity. A comparatively strong correlation with the ATP results was demonstrated using AMI quantification, indicating great significance in this non-destructive drug efficacy characterization.

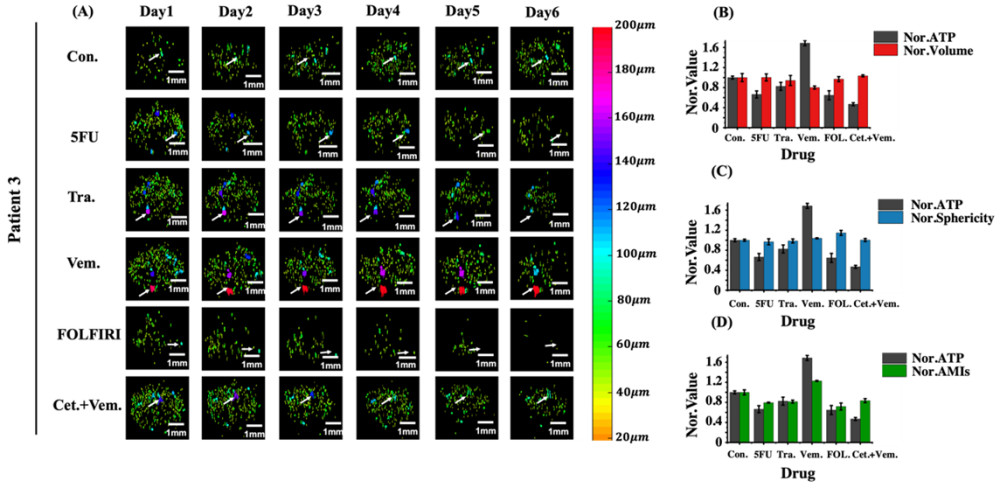

Fig. 6. OCT 3D segmentation and quantification results of P3 PDOs treated with different drugs. A: Segmented images of P3 PDOs. B-D: ATP results versus mean volume, mean sphericity and AMIs results of organoids in the single well plate at different drugs. Scale bar = 1mm. (Error bars indicate standard deviation, n = 3).

4. Discussion

Optical microscope hardly captures the variation in 3D organoid morphology to determine the drug responses of organoids. The fluorescent agents that are used as labels in fluorescence microscopy interfere with the cell environment, inhibiting the non-destructive and continuous

Biomedical Optics EXPRESS

monitoring of organoids; this problem also exists in biochemical testing [12]. Therefore, a 3D label-free imaging method is required to recognize precise morphological variations in the 3D organoid structure [6]. Consequently, OCT was adopted in this study to monitor the growth status and morphological changes induced by drugs effect on organoids (Fig. 3(A), Fig. 4(A), Fig. 5(A) and Fig. 6(A)). Compared with other imaging methods, the advantages of OCT, such as its non-destructive characteristics, deep penetration and volume imaging ability, allow evaluation of the organoids 3D variation on a continuous basis (Fig. 3(A), Fig. 4(A), Fig. 5(A) and Fig. 6(A)) [10]. In this study, the time-dependent morphological parameters of organoids were quantified using the image data acquired via OCT, this enabled investigation into the morphological variation of organoids under different drugs effect. The OCT has been implemented in several other studies for the continuous monitoring the changing status of organoid volumes under drug treatments [16].

The organoid volumetric growth trend monitored by OCT (Fig. 3) indicated that the viability and drug responses of organoids may not be accurately characterized by volume parameter only; this was concluded because the Spearman correlation coefficient between the overall volume and ATP results on the last day was determined to be < 0.8. Figure 4((B), (D)) demonstrated large discrepancies in the changing trends of the different morphological parameters under drug treatment. Specifically, the trends vary in standardized volume and standardized sphericity. Quantifying the volumetric change of organoids only and neglecting other morphological changes, such as organoid surface area or sphericity, may lead to evaluation bias. Furthermore, Gil et al. introduced multi-dimensional morphological parameters to investigate the organoids heterogeneity by cluster analysis. These results indicated that different information may be found by using multi-dimensional morphological parameters [30]. Gil et al. also investigated the estimation errors in organoid volume by calculating sphericity, which is a significant source of information in the morphological characterization of organoids [16]. Therefore, considering multiple parameters can facilitate accurate growth monitoring and drug response evaluation of organoids.

The AMIs of organoids includes volume, sphericity, quantity, and equivalent diameter [31]. Owing to OCT advantages in achieving 3D monitoring, we were able to analyze the morphological multi-parameters of organoids. Namely, we could analyze the overall volume, overall surface area, overall number, average volume, average surface area, average volume, average sphericity, average specific surface area and average equivalent diameter of each culture well at a single time point [16,17,31]. Considering the characteristics of OCT non-destructive monitoring, we were able to analyze the daily mean and time-varying standard deviation of the above parameters over 6 days. Organoid volume refers to the space occupied by an organoid, which increased over time in the control group. Under the treatments of the studied drugs, the volume tends to increase or decrease, with decreases volume attributed to the suppression of cancer organoids as a result of drug treatment. Organoid sphericity is a quantitative parameter of the organoid sphericity degree. The sphericity index of organoids enables to characterize the organoid shape, namely, whether the shape is regular or not. When the sphericity is close to 1, that means organoids are more rounded, and when it is close to 0, organoids tend to be more irregular. At the same time, we substituted the volume and surface area of organoids into the sphericity formula of organoids. Owing to volume and surface area were calculated by pixels methods, the shape of organoids can be characterized. Under drug treatment, sphericity was observed to increase or decrease over time, which may be related to the growth status of the organoids. Organoid quantity refers to the number of organoids in a particular space, and an observed increase in quantity may indicate that drug can facilitate the growth of organoids. Organoid equivalent diameter refers to the diameter of a sphere with the same volume as the organoid. Organoid equivalent diameter directly characterizes the size of the organoid and can be used to evaluate the effects of drugs on organoid size.

Biomedical Optics EXPRESS

When testing the bioactivity of colorectal cancer organoids under 5-FU treatment with different concentrations, the ATP value was found to decrease as drug concentration increased. Besides, AMIs showed a similar tend (Fig. 5(D)). Koch et al. tested the drug responses of cholangiocarcinoma organoids to various sorafenib concentrations; the corresponding results exhibited decreasing cell proliferation rates as sorafenib concentration increased [32]. Cho et al. indicated that the cancer cell survival rate and 5-FU concentration are related. Namely, the cell vitality would decrease as the drug concentration increased [4]. The reliability of the results in this study is verified by the conclusions of previous studies, and the morphological parameters of organoids under various concentrations of drug treatments were quantified. The corresponding results indicated that the AMI exhibits higher correlation with the ATP results compared to average volume and sphericity (Fig. 6(B–D)). These results were also verified by the calculated correlation coefficients. The AMI characterizes drug responses and exhibits a high degree of similarity of ATP testing. The disadvantages of ATP testing are its destructive way result in only a single-point measurement. These complications can be overcome by AMI analysis, which demonstrates potential for non-destructive, continuous, and accurate personalized drug screening.

It must be emphasized that the coefficient weight of AMIs requires re-calculation for organoids with different cancer types. In addition, there are still the discrepancies between the AMI and the of the ATP test results, which probably was attributed to the diffusion limitation of the ATP test reagent in organoids with large diameters. If the organoid radius exceeds the diffusion radius of the ATP test reagent or drug, the reagent or drug may fail to enter the organoid; therefore, this can generate errors when testing for organoid viability. The fact that organoids with a diameter < 32 μm do not possess the same functions as mature organoids, which means smaller organoids would be excluded in this study [16]. Nonetheless, as ATP is the primary carrier of energy metabolism for organoids, these deviations may lead to the discrepancies between the AMI and the ATP results [30]. However, there are some problems to be overcome when these studies can be implemented into clinical practice [33]. The next step of this investigation involves the introduction of metabolic variables or immunohistochemical analysis indicators to propose new potential AMIs for organoids. Overall, the correlation between these new AMIs and toxicological indicators can be enhanced by conducting correlation analysis between the AMI and toxicological indicators, such as ATP or MTT [8–10].

5. Conclusion

This study verifies the OCT utility as a potential imaging tool in the visualization and quantification of the 3D structural growth status of organoids. Compared with biochemical measurements, the morphological quantification in this study can provide non-destructive and continuous dynamic data of organoid growth. Compared with 2D estimation obtained from optical microscopy, the voxel-based method in calculating volume is proved to be more accurate. Continuous tracking of PDOs also indicates that different patients show different responses to drug effects, therefore personalized drug screening methods are needed. In addition, morphological parameters such as the number, volume, surface area and sphericity of organoids varied greatly under the drug effects, indicating that only considering a single morphological parameter would be isolated. Overall, AMI proposed in this report, based on PCA analysis, takes into account multi-dimensional morphological parameters of organoid clusters, thereby enhancing accuracy in drug screening and providing a novel non-destructive method by which drug effect on organoids can be quantitatively analyzed.

Biomedical Optics EXPRESS

Funding. National Key Research and Development Program of China (2022YFA1104600); National Natural Science Foundation of China (31927801); Key Research and Development Foundation of Zhejiang Province (2022C01123); Natural Science Foundation of Zhejiang Province (LQ20H100002).

Acknowledgements. This work was supported by the National Key Research and Development Program of China (2022YFA1104600), National Natural Science Foundation of China (31927801), Key Research and Development Foundation of Zhejiang Province (2022C01123) and Natural Science Foundation of Zhejiang Province (LQ20H100002).

Ethics approval and consent to participate. This study was approved by the Institutional Research Ethics Committee of the First Affiliated Hospital, College of Medicine, Zhejiang University (approval number: 2019-826). The experiments were undertaken with the understanding and written consent of each subject. This study was performed in accordance with the Declaration of Helsinki.

Disclosures. The authors declare no conflicts of interest.

Data availability. Data underlying the results presented in this paper are not publicly available at this time but may be obtained from the authors upon reasonable request.

Supplemental document. See Supplement 1 for supporting content.

References

1. M. Hofer and M. P. Lutolf, "Engineering organoids," Nat. Rev. Mater. **6**(5), 402–420 (2021).
2. W. Wu, X. Li, and S. Yu, "Patient-derived tumour organoids: a bridge between cancer biology and personalised therapy," Acta Biomater. **146**, 23–36 (2022).
3. Y. Cao and X. Wang, "Effects of molecular markers on the treatment decision and prognosis of colorectal cancer: a narrative review," J. Gastrointest. Oncol. **12**(3), 1191–1196 (2021).
4. Y.-W. Cho, D.-W. Min, H.-P. Kim, Y. An, S. Kim, J. Youk, J. Chun, J. P. Im, S.-H. Song, Y. S. Ju, S.-W. Han, K. J. Park, and T.-Y. Kim, "Patient-derived organoids as a preclinical platform for precision medicine in colorectal cancer," Molecular Oncology **16**(12), 2396–2412 (2022).
5. J. Drost and H. Clevers, "Organoids in cancer research," Nat. Rev. Cancer **18**(7), 407–418 (2018).
6. R. Keshara, Y. H. Kim, and A. Grapin-Botton, "Organoid imaging: seeing development and function," Annu. Rev. Cell Dev. Biol. **38**(1), 447–466 (2022).
7. R. K. Chhetri, Z. F. Phillips, M. A. Troester, and A. L. Oldenburg, "Longitudinal study of mammary epithelial and fibroblast co-cultures using optical coherence tomography reveals morphological hallmarks of pre-malignancy," PLoS One **7**(11), e49148 (2012).
8. V. Brancato, J. M. Oliveira, V. M. Correlo, R. L. Reis, and S. C. Kundu, "Could 3D models of cancer enhance drug screening?" Biomaterials **232**, 119744 (2020).
9. L. Makinen, M. Vaha-Koskela, M. Juusola, H. Mustonen, K. Wennerberg, J. Hagstrom, P. Puolakkainen, and H. Seppanen, "Pancreatic cancer organoids in the field of precision medicine: a review of literature and experience on drug sensitivity testing with multiple readouts and synergy scoring," Cancers **14**(3), 525 (2022).
10. H. E. Francies, A. Barthorpe, A. McLaren-Douglas, W. J. Barendt, and M. J. Garnett, "Drug sensitivity assays of human cancer organoid cultures," Methods Mol. Biol. **1576**, 339–351 (2019).
11. Y. H. Jung, D.-H. Choi, K. Park, S.-B. Lee, J. Kim, H. Kim, H.-W. Jeong, J. H. Yang, J.-A. Kim, S. Chung, and B. S. Min, "Drug screening by uniform patient derived colorectal cancer hydro-organoids," Biomaterials **276**, 121004 (2021).
12. I. A. El-Sadek, A. Miyazawa, L. T. Shen, S. Makita, P. Mukherjee, A. Lichtenegger, S. Matsusaka, and Y. Yasuno, "Three-dimensional dynamics optical coherence tomography for tumor spheroid evaluation," Biomed. Opt. Express **12**(11), 6844–6863 (2021).
13. J. Ding, Q. Li, J. Lin, S. He, W. Chen, Q. He, Q. Zhang, J. Chen, T. Wu, S. Zhong, and D. Li, "Optical coherence tomography for the early detection of colorectal dysplasia and cancer: validation in a murine model," Quant Imaging Med. Surg. **11**(1), 371–379 (2021).
14. A. J. Deloria, S. Haider, B. Dietrich, V. Kunihs, S. Oberhofer, M. Knofler, R. Leitgeb, M. Liu, W. Drexler, and R. Haindl, "Ultra-high-resolution 3D optical coherence tomography reveals inner structures of human placenta-derived trophoblast organoids," IEEE Trans. Biomed. Eng. **68**(8), 2368–2376 (2021).
15. Y. Ming, S. Hao, F. Wang, Y. R. Lewis-Israeli, B. D. Volmert, Z. Xu, A. Goestenkors, A. Aguirre, and C. Zhou, "Longitudinal morphological and functional characterization of human heart organoids using optical coherence tomography," Biosens. Bioelectron. **207**, 114136 (2022).
16. D. A. Gil, D. A. Deming, and M. C. Skala, "Volumetric growth tracking of patient-derived cancer organoids using optical coherence tomography," Biomed. Opt. Express **12**(7), 3789–3805 (2021).
17. F. Yan, G. Gunay, T. I. Valerio, C. Wang, J. A. Wilson, M. S. Haddad, M. Watson, M. O. Connell, N. Davidson, K. M. Fung, H. Acar, and Q. Tang, "Characterization and quantification of necrotic tissues and morphology in multicellular ovarian cancer tumor spheroids using optical coherence tomography," Biomed. Opt. Express **12**(6), 3352–3371 (2021).
18. L. Hof, T. Moreth, M. Koch, T. Liebisch, M. Kurtz, J. Tarnick, S. M. Lissek, M. M. A. Verstegen, L. J. W. van der Laan, M. Huch, F. Matthaus, E. H. K. Stelzer, and F. Pampaloni, "Long-term live imaging and multiscale analysis identify heterogeneity and core principles of epithelial organoid morphogenesis," BMC Biol. **19**(1), 37 (2021).

Biomedical Optics EXPRESS

19. M. G. Fakih, "Trastuzumab Plus pertuzumab resistance does not preclude response to lapatinib plus trastuzumab in HER2-amplified colorectal cancer," Oncologist. **23**(4), 474–477 (2018).
20. D. S. Hong, V. K. Morris, and B. El Osta, *et al.*, "Phase IB study of vemurafenib in combination with irinotecan and cetuximab in patients with metastatic colorectal cancer with BRAFV600E mutation," Cancer Discovery **6**(12), 1352–1365 (2016).
21. R. Cao, S. Zhang, D. Ma, and L. Hu, "A multi-center randomized phase II clinical study of bevacizumab plus irinotecan, 5-fluorouracil, and leucovorin (FOLFIRI) compared with FOLFIRI alone as second-line treatment for Chinese patients with metastatic colorectal cancer," Med. Oncol. **32**(1), 325 (2015).
22. S. Kopetz, K. A. Guthrie, and V. K. Morris, *et al.*, "Randomized trial of irinotecan and cetuximab with or without vemurafenib in BRAF-mutant metastatic colorectal cancer (SWOG S1406)," J. Clin. Oncol. **39**(4), 285–294 (2021).
23. E. Bigaeva, J. J. M. Bomers, C. Biel, H. A. M. Mutsaers, I. A. M. de Graaf, M. Boersema, and P. Olinga, "Growth factors of stem cell niche extend the life-span of precision-cut intestinal slices in culture: A proof-of-concept study," Toxicol. In Vitro **59**, 312–321 (2019).
24. J. Motoyoshiya, J. Y. Wada, K. Itoh, K. Wakabayashi, T. Maruyama, K. Ono, K. Fukasawa, T. Fujimoto, Y. Akaiwa, and E. Nonaka, "Fluorescence and chemiluminescence behavior of distyrylbenzene bearing two arms of dipicolylaminomethyl groups: Interactions with zinc ion and ATP," Spectrochim. Acta, Part A **195**, 223–229 (2018).
25. M. A. Borten, S. S. Bajikar, N. Sasaki, H. Clevers, and K. A. Janes, "Automated brightfield morphometry of 3D organoid populations by OrganoSeg," Sci. Rep. **8**(1), 5319 (2018).
26. H. Luo, S. Li, Y. Zeng, H. Cheema, E. Otegbeye, S. Ahmed, W. C. Chapman Jr., M. Mutch, C. Zhou, and Q. Zhu, "Human colorectal cancer tissue assessment using optical coherence tomography catheter and deep learning," J. Biophotonics **15**(6), e202100349 (2022).
27. M. A. Foo, M. You, S. L. Chan, G. Sethi, G. K. Bonney, W. P. Yong, E. K. Chow, E. L. S. Fong, L. Wang, and B. C. Goh, "Clinical translation of patient-derived tumour organoids- bottlenecks and strategies," Biomark. Res. **10**(1), 10 (2022).
28. Z. Chen, N. Ma, X. Sun, Q. Li, Y. Zeng, F. Chen, S. Sun, J. Xu, J. Zhang, H. Ye, J. Ge, Z. Zhang, X. Cui, K. Leong, Y. Chen, and Z. Gu, "Automated evaluation of tumor spheroid behavior in 3D culture using deep learning-based recognition," Biomaterials **272**, 120770 (2021).
29. Y. Qin, J. Wang, Y. Han, and L. Lu, "Deep learning algorithms-based CT images in glucocorticoid therapy in asthma children with small airway obstruction," J. Healthc. Eng. **2021**, 5317403 (2021).
30. N. Y. Chun, S.-N. Kim, Y. S. Choi, and Y. B. Choy, "PCN-223 as a drug carrier for potential treatment of colorectal cancer," J. Ind. Eng. Chem. **84**, 290–296 (2020).
31. D. A. Gil, D. Deming, and M. C. Skala, "Patient-derived cancer organoid tracking with wide-field one-photon redox imaging to assess treatment response," Biomed. Opt. Express **26**(3), 1 (2021).
32. X. Yu, A. M. Fuller, R. Blackmon, M. A. Troester, and A. L. Oldenburg, "Quantification of the effect of toxicants on the intracellular kinetic energy and cross-sectional area of mammary epithelial organoids by OCT fluctuation spectroscopy," Toxicol. Sci. **162**(1), 234–240 (2018).
33. M. Koch, S. Nickel, R. Lieshout, S. M. Lissek, M. Leskova, L. J. W. van der Laan, M. M. A. Verstegen, B. Christ, and F. Pampaloni, "Label-free imaging analysis of patient-derived cholangiocarcinoma organoids after sorafenib treatment," Cells **11**(22), 3613 (2022).
34. D. Bao, L. Wang, X. Zhou, S. Yang, K. He, and M. Xu, "Automated detection and growth tracking of 3D bio-printed organoids population using optical coherence tomography with deep convolutional neural networks," (In submission).